Russian Journal of Earth Sciences, Vol. 22, ES6013
https://doi.org/10.2205/2022ES000832

Geographical and seasonal distribution of tidal body force field in the Sea of Okhotsk in the context of internal wave dynamics

M. V. Kokoulina[1], O. E. Kurkina[1], E. A. Rouvinskaya[1], and A. A. Kurkin*[,1]

[1] *Nizhny Novgorod State Technical University n. a. R. E. Alekseev, Nizhny Novgorod, Russia*

Received 25 October 2022; accepted 4 November 2022; published 31 December 2022.

Estimates of the barotropic tidal body force for diurnal and semidiurnal tides are obtained for the Sea of Okhotsk for the summer and winter periods. It is shown that in the study area, the tidal body force for diurnal tides is significantly greater than for semidiurnal ones. The maximum values of this quantity can reach about 2–8 $m^2 s^{-2}$, and these values are typical for areas with a sharp bathymetric gradient. A comparison of the tidal body force for the two seasons showed noticeable differences. The features of the transformation of a barotropic tidal wave propagating in the zone of large values of the tidal body force for the K_1, O_1, M_2 tidal constituents are demonstrated. Numerical simulations indicate that baroclinic tidal waves are effectively generated in this area, and intense short-period internal waves are likely to occur.

Keywords: Sea of Okhotsk, tidal body force, multicomponent barotropic tide, internal waves, numerical modeling.

Citation: Kokoulina, M. V., O. E. Kurkina, E. A. Rouvinskaya, and A. A. Kurkin, (2022), Geographical and seasonal distribution of tidal body force field in the Sea of Okhotsk in the context of internal wave dynamics, *Russian Journal of Earth Sciences*, Vol. 22, ES6013, doi: 10.2205/2022ES000832.

1 Introduction

The generation of internal tides is closely related to the action of the body force that occurs when a barotropic tidal flow goes around bottom roughness. It emerges in the right-hand side of the equation of motion for the vertical velocity component and actually determines the tidal forcing. In fact, this quantity determines the barotropic to baroclinic transfer of tidal energy [*Gustafsson*, 2001]. Knowledge of the spatial distribution and seasonal variations of the tidal body force in a particular water area makes it possible to identify possible zones of more efficient generation of internal tides. This is necessary for the correct adjustment of computational models of marine dynamics, for zoning currents and related impacts on underwater objects and marine ecosystems, for planning human activities, in particular, for assessing risks in the design of hydraulic structures on the shelf. The constructed maps can be used along with maps of the Rossby baroclinic radius, as well as maps of kinematic, dispersion and nonlinear parameters of long short-period internal waves [*Kurkina et al.*, 2017a,b,c; *Rouvinskaya et al.*, 2018; *Stepanov*, 2017] for preliminary estimates of possible effects, including planning numerical experiments.

The spatial distribution of the tidal body force is often used to determine the location of possible internal wave generation zones in various regions of the World Ocean [*Bai et al.*, 2014; *da Silva et al.*, 2007; *Lozovatsky et al.*, 2011; *Magalhaes and da Silva*, 2012; *Pichon et al.*, 2013; *Sherwin et al.*, 2002; *Vlasenko et al.*, 2014; *Wang et al.*, 2022; *Zhao et al.*, 2021]. For example, in [*Wang et al.*, 2022], the calculation of the body tidal force for the South China Sea for the M_2 and K_1 tidal components is presented and it is shown that the semidiurnal tidal body force is significantly greater than that for diurnal tides in the considered water area. Typical values for this quantity, as a rule, do not exceed $10\,m^2 s^{-2}$, but can reach few tens of $m^2 s^{-2}$ for certain geographical areas with extreme tides, such as the Celtic Sea shelf break [*Vlasenko et al.*, 2014].

In this article we aim at the clarification of spatial distribution of the tidal body force in the Sea of Okhotsk for three main tidal components K_1, O_1 and M_2. These distributions reflect not only

*Corresponding author: aakurkin@nntu.ru

geographic variability of bathymetry and water masses of this basin but also mirror strong seasonal variations in the atmospheric and hydrographic features in the region.

The structure of the paper is as follows. Section 2 presents the details of the calculations and sources of the data. A short insight into the common concept of tide structure in the study area is presented in section 3. The seasonal and spatial variability of the barotropic tidal body force is discussed in detail in section 4. A selection of results of numerical simulation of barotropic tide transformation into baroclinic motions along a section in the northern part of the eastern shelf of Sakhalin Island is described in section 5. The closing section 6 provides a short discussion of the main results.

2 Details of the calculation and data used

The formula for calculating the barotropic tidal body force was used following the works [*Baines*, 1973, 1982]:

$$F = -\frac{\vec{Q}\nabla H}{\omega H^2}\int_{-H}^{0} zN^2(z)dz, \qquad (1)$$

where z indicates the vertical location, $\vec{Q}$ is the barotropic tidal volume transport for the corresponding tidal component, H is the local sea depth, ∇H is the bottom gradient, ω is corresponding tidal frequency, $N(z)$ is the Brunt–Väisälä frequency. Its profiles have been calculated using the standard approach based on the classic definition:

$$\mathrm{N}^2(z) = -\frac{g}{\rho_0(z)}\frac{d\rho_0(z)}{dz}. \qquad (2)$$

Here g is acceleration due to gravity and $\rho_0(z)$ represents the vertical variation in water density.

The international hydrological atlas WOA18, the bathymetry array GEBCO, and the output of the tidal model TPXO8 were used as initial data.

Generalised and standardised information about the basic features of hydrophysical parameters of sea water and their seasonal variations has been integrated into the open source digital climatologic atlas World Ocean Atlas 2018 (WOA18). It provides arrays of averaged and smoothed data of field measurements for temperature, salinity and other hydrological parameters [*Boyer et al.*, 2018]. The information in WOA18 is gridded to a regular rectangular set with a horizontal resolution of 5°, 1° or 1/4°. Data that represent the vertical profiles of temperature and salinity are yearly, seasonally and monthly averaged at 137 vertical levels. In this study, we used salinity and temperature data for summer and winter periods, on the basis of which, using the equation of state of sea water TEOS10 (http://teos-10.org/), we reconstructed the potential density of sea water and calculated the Brunt–Väisälä frequency, Eq. (2).

GEBCO (https://www.gebco.net/) is a digital atlas of ocean bathymetry. We have used the latest GEBCO-2022, which contains a bathymetry dataset with a resolution of 15 arcseconds.

Maximum tidal flux data for main tidal components were taken from the TPXO 8 (A TOPEX/Poseidon Global Tidal Model) tidal model based on satellite altimetry data [*Egbert and Erofeeva*, 2002].

All atlases had different data formats and grid resolutions, so the calculations required their initial processing. Bathymetry gradient vector ∇H was calculated on the original GEBCO grid. All data were then interpolated to the coarsest grid, and the resulting array of tidal body force values is presented on a grid which horizontal resolution is determined by the spatial resolution of the WOA18 atlas input (1/4 degree).

3 Structure of the tide in the Sea of Okhotsk

Tidal phenomena in the Sea of Okhotsk are associated with the propagation of a tidal wave from the Pacific Ocean through the straits of the Kuril chain. They cause significant fluctuations in sea level, speed and direction of currents. According to the nature of the level fluctuations, all types of tides are manifested here to varying degrees: semidiurnal, irregular semidiurnal, irregular diurnal and diurnal. The dynamics of long-wave processes, especially on the northeastern shelf of the Sakhalin Island, is determined primarily by the features of the tidal regime. The study of currents at the Odoptinskaya, Piltun-Astokhskaya and Veninskaya sites made it possible to identify the shelf wave (a kind of topographic Rossby waves) in the daily K_1 and O_1 waves [*Rabinovich and Zhukov*, 1984]. The complex nature of tidal and shelf wave propagation off the eastern coast of Sakhalin Island, their intra-annual and inter-annual variability (according to field observations), as well as significant spatial variability of the harmonic constants of the main tidal waves [*Deyeva*, 1972; *Putov and Shevchenko*, 1998; *Shevchenko*, 1996] make these processes an inconvenient object for numerical simulation [*Kowalik and Polyakov*, 1998], since it is necessary to take into account as much as possible the available information on the values of harmonic constants at various points in the simulation area. The largest contribution to the tidal flow in the Sea of Okhotsk is made by harmonics K_1, the lunisolar declinary

diurnal component, O_1, the main lunar diurnal wave, and M_2, the main lunar semidiurnal component. In this case, it is possible to conditionally distinguish areas with different ratios of the main components (Figure 1). Diurnal, semidiurnal and irregular diurnal tides are mostly observed in the study area. [*Moroz et al.*, 2010].

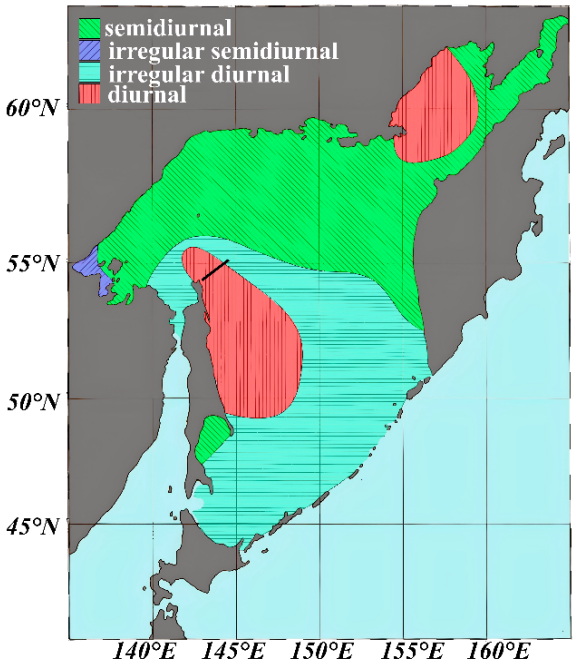

Figure 1: Mapping of the Sea of Okhotsk according to the types of complex tides with different ratios of the main components. Adapted from [*Moroz et al.*, 2010]. The black line near the north-eastern coast of Sakhalin Island shows the location of the cross-section for the analysis in section 5.

4 Results of tidal body force calculations

As described above, from knowledge of the density distribution, tidal volume transport and bottom bathymetry discretized on a rectangular grid, the value of tidal body force at each grid segment can be calculated. At the same time, analyzing the expression Eq. (1), one can see that, ceteris paribus, the value of F reaches its maximum values when the bottom depth gradient is large and its direction is close to (collinear with) the tidal flux vector. Seasonal changes in Eq. (1) are presented through the integral multiple, which is determined by the seawater density stratification. The detailed analysis of spatial and seasonal variations in the density-driven stratification in the Sea of Okhotsk and their impact on the properties of short-period nonlinear internal waves in this water body is given in [*Kurkina et al.*, 2017c]. It was shown that the vertical structure of water masses of the Sea of Okhotsk exhibits substantial seasonal variations. The maxima of $N(z)$ in summer are, on average, four times as large as the relevant maxima in winter. This should provide a noticeable difference in tidal body force calculated for different seasons.

The computed spatial distributions of F (1) in the Sea of Okhotsk are characterized by average values of the order of $0.02\,m^2\,s^{-2}$ in case of M_2 component, or $0.07\,m^2\,s^{-2}$ for K_1 tidal constituent, see Table 1 for details (note, that the estimates in Table 1 are given for the whole rectangular geographical region shown further in

However, the median of F is much lower than the mean, around $0.005–0.006\,m^2\,s^{-2}$ for M_2 and for K_1, indicating a highly positively skewed distribution. As much as 80% of the values of F are less than the mean for all tidal components and seasons. In terms of total forces, for example, less than only 16% of the area contributes to more than 63% of the total barotropic tidal forcing for K_1 tide. Similar estimates for other tidal components for different seasons are given in Table 1

The geographical distribution of F (Figure 2–Figure 4) show strongly enhanced forcing of the baroclinic tide in areas of steep topography, such as shelf and through slopes. Figure 2a, b shows the spatial distribution of F, Eq. (1), for the Sea of Okhotsk for the tidal component K_1. The maximum values are distributed near the Kuril Islands, along the perimeter of the Kuril Basin, and to the north of Sakhalin Island, over the Deryugin Basin. These areas are characterized by sharp bathymetric gradients. It should be noted that in the area of the shelf of the Kamchatka Peninsula, many discrete areas were also found where the values of the tidal body force are high. Figure 2b shows that in winter in some areas the tidal body force values decrease, for example, this is typical for the Gulf of Sakhalin, the Penzhina Bay area, and the La Perouse Strait. On the other hand, in winter, the areas of high values in the vicinity of the Kuril Basin even slightly expand.

Similar calculations for two seasons were carried out for the O_1 tidal component (Figure 3a, b). Since the values of the maximum tidal flux for the K_1 and O_1 harmonics are similar, which was also noted in [*Putov and Shevchenko*, 1998], the tidal body force values for these components, as well as the spatial distribution and seasonal variability, almost do not differ qualitatively. The quantitative difference is small, but still noticeable, including in the estimates given in Table 1. The body force values for the O_1 tide are generally slightly lower, than those for K_1.

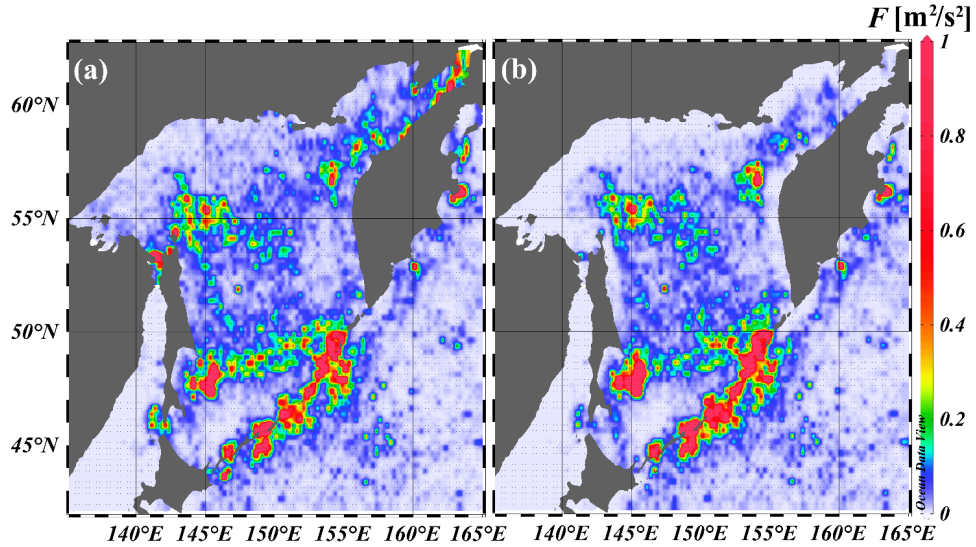

Figure 2: Tidal body forces for diurnal (K_1) tides in (a) summer and (b) winter. These and other maps in this paper are drawn using Ocean Data View software [*Schlitzer*, 2022].

For the M_2 component, the spatial distribution of the tidal body force for summer and winter is shown in Figure 4a, b, respectively. In comparison with the considered results for the K_1 and O_1 components in the study area, the semidiurnal tidal body force is significantly less than that for diurnal tides. The maximum values of F for M_2 are also distributed near the Kuril Islands, along the perimeter of the Kuril Basin, and, for the summer season Figure 4a, it is still possible to distinguish areas of large values in the Gulf of Sakhalin and in the Penzhina Bay.

As mentioned above, the difference in the spatial distributions of the tidal force between the diurnal and semidiurnal components is very significant, which is confirmed by Figure 5, where the relative difference for the pairs of tidal components in the form

$$\delta_{K_1M_2} = 100 \times \frac{\left|F_{K_1} - F_{M_2}\right|}{F_{M_2}} \qquad (3)$$

is mapped for the summer season. The relative difference of tidal body force values for pairs (K_1, M_2) and (O_1, M_2) exceeds 100% in a very significant part of the Sea of Okhotsk.

In shallow water areas, the values of the tidal force are very sensitive to the season. This is clearly seen from Figure 6 which shows the relative difference between the tidal body force in summer and winter for the K_1 tidal component in the Sea of Okhotsk. For the O_1 and M_2 components, the result is the same, since when calculating the relative difference $\delta_{s,w}$, only the integral factors remain, determined by the seawater density stratification

$$\begin{aligned}\delta_{s,w} &= 100 \times \frac{|F_{sum} - F_{win}|}{(F_{sum} + F_{win})/2} \\ &= 100 \times \frac{\int_{-H}^{0} z\left|N^2_{sum}(z) - N^2_{win}(z)\right| dz}{\int_{-H}^{0} z\left(N^2_{sum}(z) + N^2_{win}(z)\right) dz/2}.\end{aligned} \qquad (4)$$

The most pronounced relative seasonal variations are observed in depths up to 1000 m. Ab-

Table 1: Characteristics of the tidal body force spatial distribution for different tidal components for summer and winter seasons

		F_{max} [$m^2 s^{-2}$]	F_{mean} [$m^2 s^{-2}$]	F_{median} [$m^2 s^{-2}$]	% of the area, where $F<F_{mean}$	% of the total barotropic tidal forcing for values $F>0.1$ $m^2 s^{-2}$	% of the area, where $F>0.1$ $m^2 s^{-2}$
K_1	summer	8.18	0.08	0.015	82.8	63.7	15.8
	winter	8.08	0.07	0.011	83.2	61.8	14.5
O_1	summer	7.43	0.06	0.011	83.4	60.2	13.7
	winter	6.40	0.06	0.009	84.2	53.3	7.2
M_2	summer	1.70	0.02	0.007	78.9	38.8	3.5
	winter	2.33	0.02	0.005	81.7	39.9	3.7

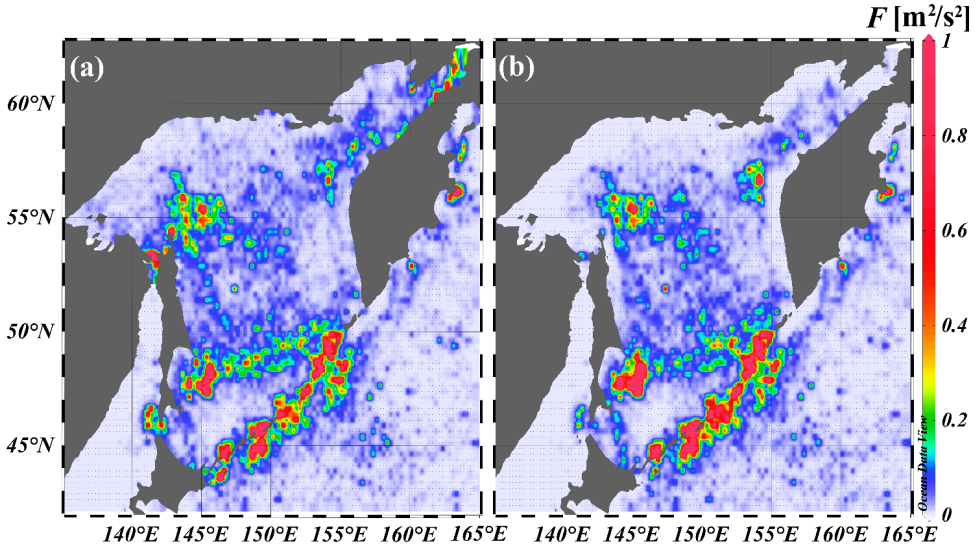

Figure 3: Tidal body forces for diurnal (O_1) tides (a) summer and (b) winter.

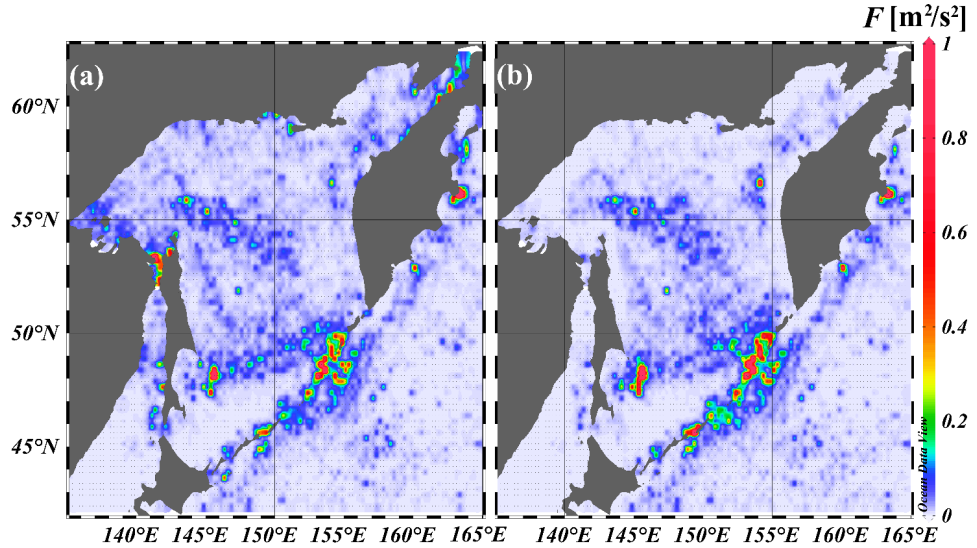

Figure 4: Tidal body forces for semidiurnal (M_2) tides in (a) summer and (b) winter.

solute differences of F values for different seasons, determined by the following expression

$$\begin{aligned}\Delta_{s,w} &= |F_{sum} - F_{win}| \\ &= \left| \frac{-\vec{Q}\nabla H}{\omega H^2} \left(\int_{-H}^{0} z {N_{sum}}^2(z) dz \right. \right. \\ &\quad \left. \left. - \int_{-H}^{0} z {N_{win}}^2(z) dz \right) \right|,\end{aligned} \tag{5}$$

reach maximum values in the same areas where the values of the compared values are high (Figure 7).

To build the maps of tidal body force values for various tidal components, a software package with a graphic user interface has been developed [*Kokoulina et al.*, 2022], and this desktop application is available upon a request from the authors.

5 DYNAMICS OF BAROCLINIC WAVE MOTIONS IN A ZONE OF LARGE VALUES OF THE TIDAL BODE FORCE

To demonstrate some applications of the constructed maps of tidal body force, we consider the process of formation of internal waves from barotropic tide in typical conditions of the northeastern shelf of Sakhalin and the adjacent continental slope in summer season. The selected cross-section (Figure 1) passes from the zone of large body force values for the K_1, O_1, M_2 tidal components (in the Deryugin Basin) towards the coast (towards the Schmidt Peninsula near Cape Elizaveta) through the Deryuginsky and North Sakhalin oil and gas basins and belongs to the Sakhalin-5 block. Numerical simulation of the generation and dynamics of baroclinic waves was performed using

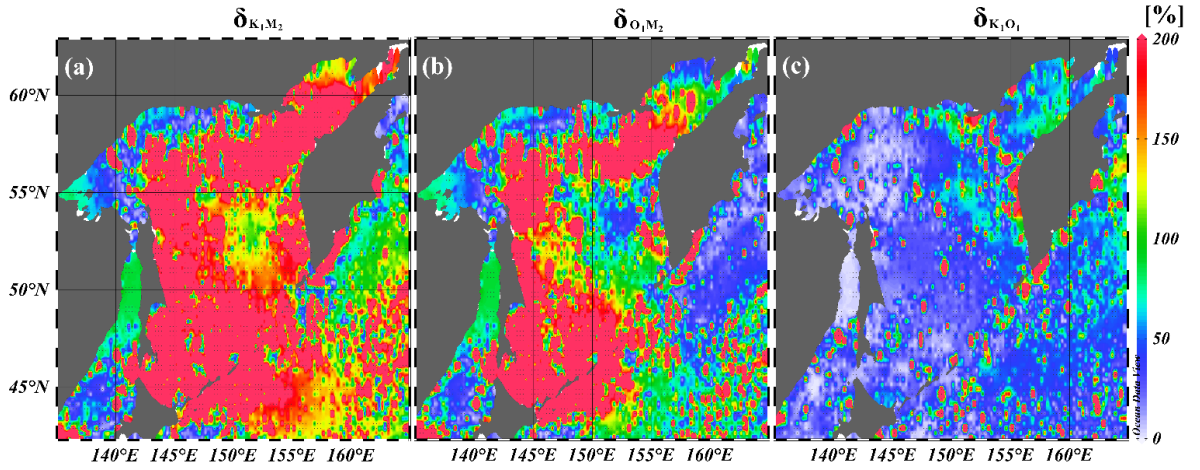

Figure 5: Relative value of difference between tidal body forces for different tidal constituents in the Sea of Okhotsk in summer: (a) K_1 and M_2, (b) O_1 and M_2, (c) K_1 and O_1.

a software package that implements the procedure for numerical integration of a fully nonlinear two-dimensional (vertical plane) hydrodynamic equations for an inviscid incompressible stratified rotating fluid in the Boussinesq approximation, taking into account the influence of the barotropic tide [*Lamb*, 1994]. A description of the model, as well as a comparison of the simulation results with field measurements, can be found in our works, including those devoted to the study of the dynamics of internal waves in the Sea of Okhotsk [e.g., *Kuznetsov et al.*, 2021; *Rouvinskaya et al.*, 2017, 2021]. To initialize the calculations, the bottom relief functions were parametrized based on the GEBCO-2022 data and density stratification from the climatological atlas WOA18; data on the amplitudes and phases of the multicomponent barotropic tide were taken from the TPXO8 model. The bottom relief along the considered transect is shown in Figure 8. The variations in the Brunt–Väisälä frequency $N(z)$ (also shown in Figure 8) are moderate in the entire water column along this profile, the maximum values of this quantity reach up to 0.05 s^{-1} in summer.

It is well known that a barotropic tide that propagates from the deep sea into stratified water masses on the continental slope often transforms into a baroclinic tide [*Vlasenko et al.*, 2005]. The dynamics of internal waves in the region under study corresponds to the classical scheme of the transformation of long barotropic tidal waves into baroclinic ones, followed by the formation of wave bores and intense short-period internal waves. In typical conditions of summer the onset of formation of internal bores from the baroclinic tidal wave is located at a distance of approximately 90 km from the origin of the transect Figure 9. The generation zones are determined by the resonant combination of the bottom slope, the Brunt-Väisälä

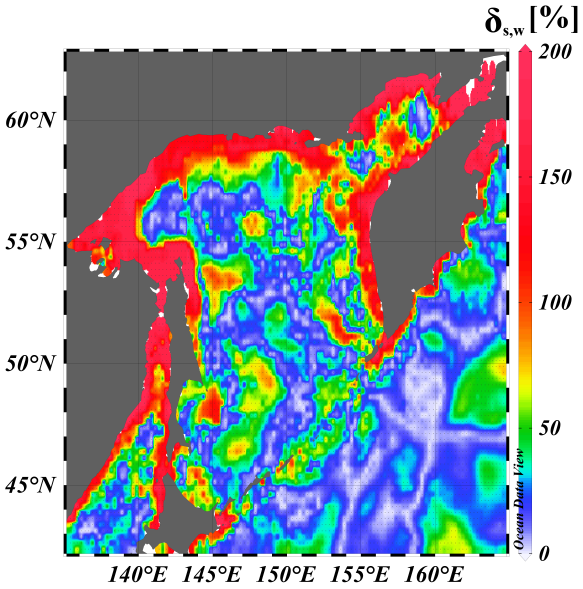

Figure 6: Spatial distribution of the relative difference $\delta_{s,w}$ between tidal body force values for summer and winter for any tidal component.

frequency, and the tidal forcing frequency [*Baines*, 1995]. The emerging steep fronts, propagating on- and off-shore from the critical zones, further transform into short-period solitary internal waves and their trains. The amplitudes of long baroclinic waves of tidal periods are 10–15 m, short-period waves also have amplitudes about 10 m in the field of density isolines displacement (Figure 9 and Figure 10).

The linear theory of the baroclinic tides predicts that baroclinic waves of frequency ω cannot propagate as free waves to the north of the critical latitude φ, where the tidal frequency ω is equal to the local inertial frequency $f = 2\Omega_E \sin\varphi$, where $\Omega_E = 0.00007292\ s^{-1}$ is the frequency of the Earth's

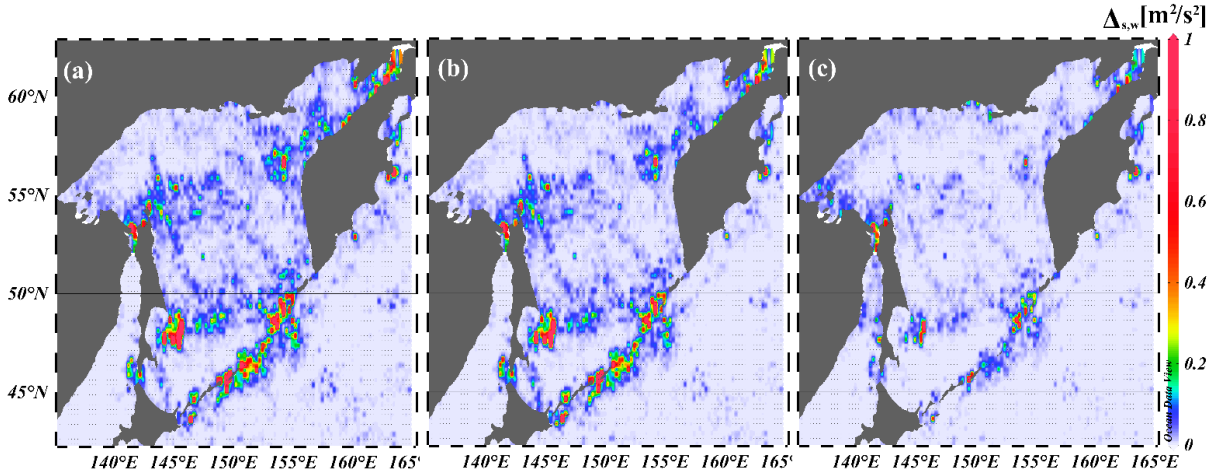

Figure 7: Absolute difference $\Delta_{s,w}$ between tidal body force values for summer and winter in the Sea of Okhotsk: (a) for K_1, (b) for O_1, (c) for M_2.

rotation [*LeBlond and Mysak*, 1978]. This latitude for tidal period $T_{M_2} = 12.4$ h is 75°, and only about 30° for the diurnal tidal periods. However, diurnal baroclinic waves in the Sea of Okhotsk can be generated locally and propagate as lee waves; due to the nonlinear generation of higher harmonics, which can propagate freely, highly nonlinear small-scale internal waves are excited. Thus, the typical tidal, hydrological and bathymetric conditions of the Sea of Okhotsk can drive complicated patterns of internal wave fronts and intense short-period waves as well as the induced baroclinic flows of complex structure (Figure 11) in the nearshore of the Sakhalin Island. Figure 11 shows the vertical distribution of the exceedance probabilities for the horizontal velocity levels in the orbital motion of fluid particles at different points of the path for the considered section. The horizontal velocity field characterized by Figure 11 is essentially vertically inhomogeneous at all horizontal locations, while the velocity in a barotropic tide does not change with depth. The asymmetry of the distributions at the bottom and on the surface is also noticeable, where, obviously, the maximum velocity values are achieved. At the same time, there are specific layers in the middle of the water column at which the velocities are always close to zero, and above and below them there are multidirectional flows. Asymmetry is also observed in horizontal (in on-, off- shore flows). All this indicates a complex nonlinear multimodal structure of baroclinic wave fields and induced shear flows.

6 Conclusions

Maps of the spatial distribution of the tidal body force in the Sea of Okhotsk were constructed for the main tidal components K_1, O_1, M_2 for winter

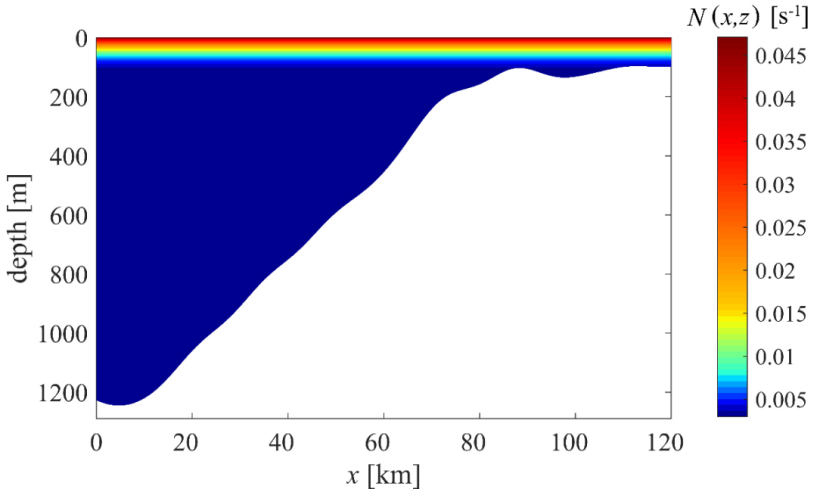

Figure 8: Characteristic vertical structure of the Brunt–Väisälä frequency in summer along the cross-section.

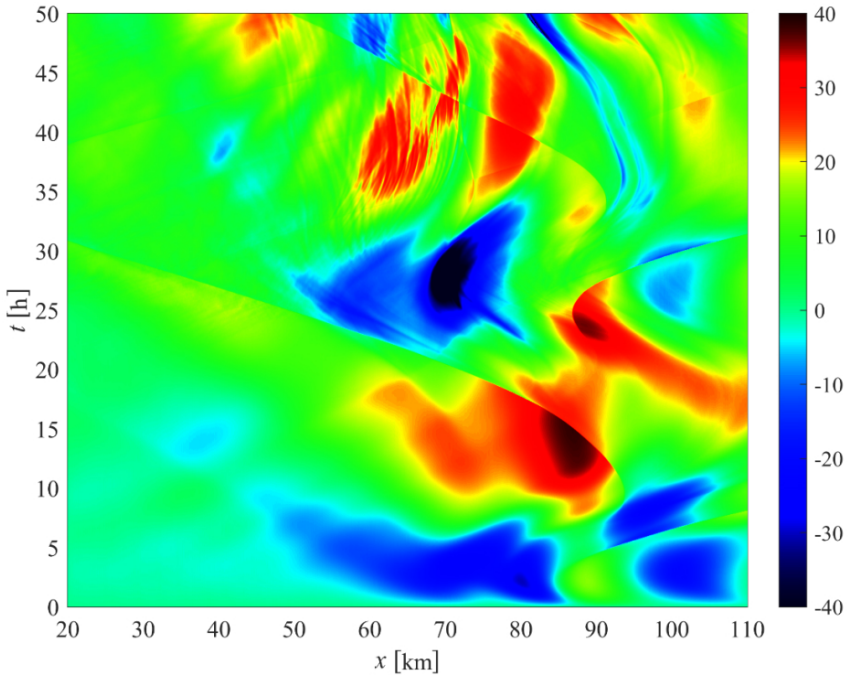

Figure 9: Evolution of a baroclinic tide along the transect: space-time (x–t) diagram of the deviations of isopycnal surfaces (colour scale, m) from their undisturbed horizon $z = 70$ m.

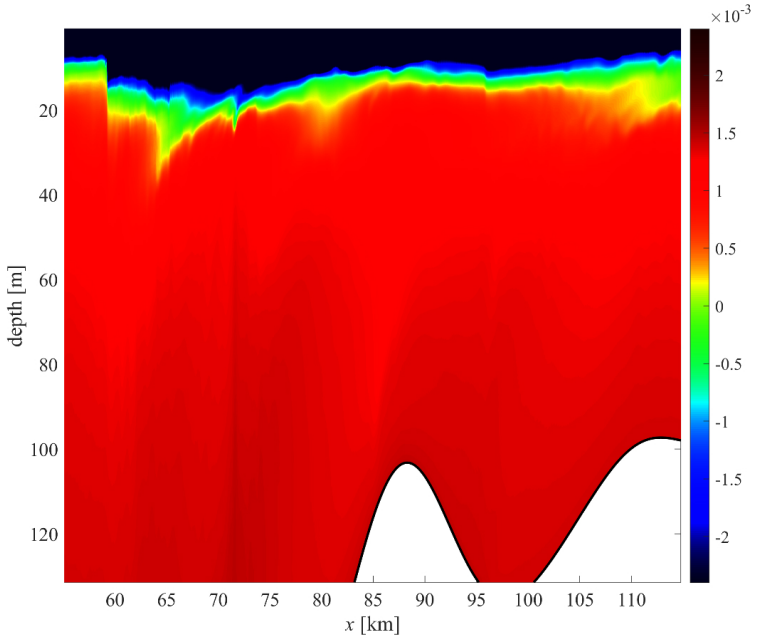

Figure 10: Snapshot of the simulated normalized density anomaly field demonstrating various generated waveforms: long baroclinic waves, steep wave fronts and large-amplitude short-period waves.

and summer seasons. The diurnal tidal body force is significantly greater than the force for semidiurnal tides almost everywhere in the studied region. Characteristic values of body force for the Sea of Okhotsk do not exceed 2–8 $m^2 s^{-2}$. The maximum values of this value are typical for areas with a sharp bathymetric gradient. It is shown that the seasonal change in seawater density stratification evidently affects the spatial distribution and the magnitude of the tidal body force. In all cases, the median of the tidal body force is less than its individual mean and all distributions of F are positively skewed, indicating that a small fraction of the area is responsible for the bulk of the possi-

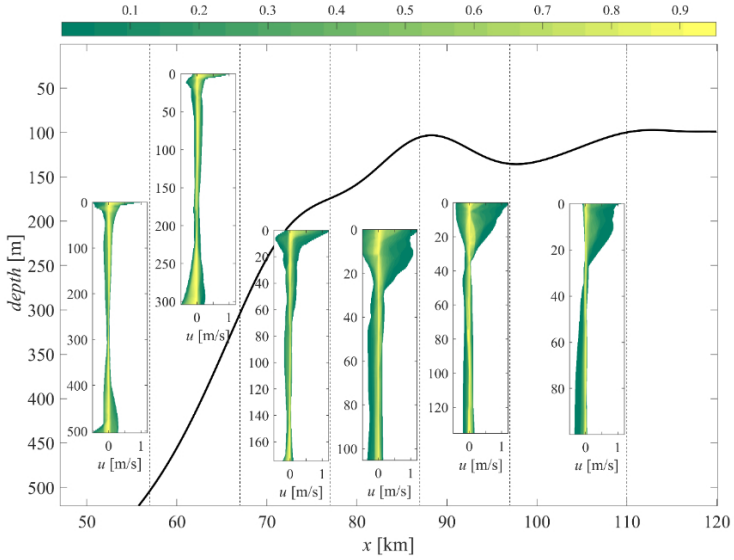

Figure 11: Frequency of occurrence of large flow velocity values along the *z*-axis at different locations (marked by vertical dashed lines) along the cross-section. Colors indicate the exceedance probability for velocity levels.

ble total energy transfer from barotropic to baroclinic motions. The features of the transformation of a tidal wave propagating from the zone of large values of the barotropic tidal body force for the components K_1, O_1, M_2 are demonstrated. It is shown that in this area long internal waves of tidal periods are generated with amplitudes of 5–15 m, and the intense short-period internal waves appear every diurnal period. The time evolution of the horizontal velocity field was also modeled, and significant values of flow velocities are obtained, with the maximal values greater than the amplitude of the barotropic tidal flow.

Acknowledgements. The reported study was funded by the Ministry of Science and Higher Education of the Russian Federation (project No. FSWE-2020-0007) and the Council of the grants of the President of the Russian Federation for the state support of Leading Scientific Schools of the Russian Federation (Grant No. NSH-70.2022.1.5) and young scientists and graduate students (Grant No. SP-692.2021.5).

References

Bai, X., Z. Liu, X. Li, and J. Hu (2014), Generation sites of internal solitary waves in the southern Taiwan Strait revealed by MODIS true-colour image observations, *International Journal of Remote Sensing*, *35*(11–12), 4086–4098, doi:10.1080/01431161.2014.916453.

Baines, P. G. (1973), The generation of internal tides by flat-bump topography, *Deep Sea Research and Oceanographic Abstracts*, *20*(2), 179–205, doi:10.1016/0011-7471(73)90050-8.

Baines, P. G. (1982), On internal tide generation models, *Deep Sea Research Part A. Oceanographic Research Papers*, *29*(3), 307–338, doi:https://doi.org/10.1016/0198-0149(82)90098-X.

Baines, P. G. (1995), *Topographic effects in stratified flows*, 558 pp., Cambridge University Press, Cambridge.

Boyer, T. P., H. E. García, R. A. Locarnini, M. M. Zweng, et al. (2018), World Ocean Atlas 2018. Temperature, Salinity, *NOAA National Centers for Environmental Information. Dataset*, https://www.ncei.noaa.gov/access/metadata/landing-page/bin/iso?id=gov.noaa.nodc:NCEI-WOA18, Accessed: 08.08.2022.

da Silva, J. C., A. L. New, and A. Azevedo (2007), On the role of SAR for observing "local generation" of internal solitary waves off the Iberian Peninsula, *Canadian Journal of Remote Sensing*, *33*(5), 388–403, doi:10.5589/m07-041.

Deyeva, R. A. (1972), Catalog of harmonic and non-harmonic constant tides of domestic waters of the Far East, *Trudy DVNIGMI*, (18), 248, (in Russian).

Egbert, G. D., and S. Y. Erofeeva (2002), Efficient Inverse Modeling of Barotropic Ocean Tides, *Journal of Atmospheric and Oceanic Technology*, *19*(2), 183–204, doi:10/bh84s5.

Gustafsson, K. E. (2001), Computations of the energy flux to mixing processes via baroclinic wave drag on barotropic tides, *Deep Sea Research Part I: Oceanographic Research Papers*, *48*(10), 2283–2295, doi:10.1016/s0967-0637(01)00008-5.

Kokoulina, M. V., O. E. Kurkina, E. A. Rouvinskaya, and A. A. Kurkina (2022), Certificate of state registration of computer programs no 2022663958 "software package for calculating the body force in a stratified

sea with an uneven bottom based on international atlases and models", RF. 09.08.2022.

Kowalik, Z., and I. Polyakov (1998), Tides in the Sea of Okhotsk, *Journal of Physical Oceanography*, *28*(7), 1389–1409, doi:10/cp3x47.

Kurkina, O., E. Rouvinskaya, T. Talipova, and T. Soomere (2017a), Propagation regimes and populations of internal waves in the Mediterranean Sea basin, *Estuarine, Coastal and Shelf Science*, *185*, 44–54, doi:10.1016/j.ecss.2016.12.003.

Kurkina, O., T. Talipova, T. Soomere, A. Giniyatullin, and A. Kurkin (2017b), Kinematic parameters of internal waves of the second mode in the South China Sea, *Nonlinear Processes in Geophysics*, *24*(4), 645–660, doi:10.5194/npg-24-645-2017.

Kurkina, O. E., T. G. Talipova, T. Soomere, A. A. Kurkin, and A. V. Rybin (2017c), The impact of seasonal changes in stratification on the dynamics of internal waves in the Sea of Okhotsk, *Estonian Journal of Earth Sciences*, *66*(4), 238–255, doi:10.3176/earth.2017.20.

Kuznetsov, P. D., E. A. Rouvinskaya, O. E. Kurkina, and A. A. Kurkin (2021), Transformation of baroclinic tidal waves in the conditions of the shelf of the far eastern seas, in *IOP Conference Series: Earth and Environmental Science*, vol. 946, p. 012024, IOP Publishing, doi:10.1088/1755-1315/946/1/012024.

Lamb, K. G. (1994), Numerical experiments of internal wave generation by strong tidal flow across a finite amplitude bank edge, *Journal of Geophysical Research: Oceans*, *99*(C1), 843–864, doi:10.1029/93JC02514.

LeBlond, P. H., and L. A. Mysak (1978), *Waves in the Ocean*, Elsevier Oceanography Series 20, Elsevier.

Lozovatsky, I., Z. Liu, H. Fernando, J. Armengol, and E. Roget (2011), Shallow water tidal currents in close proximity to the seafloor and boundary-induced turbulence, *Ocean Dynamics*, *62*(2), 177–191, doi:10.1007/s10236-011-0495-3.

Magalhaes, J. M., and J. C. B. da Silva (2012), SAR observations of internal solitary waves generated at the Estremadura Promontory off the west Iberian coast, *Deep Sea Research Part I: Oceanographic Research Papers*, *69*, 12–24, doi:10.1016/j.dsr.2012.06.002.

Moroz, V. V., K. T. Bogdanov, V. I. Rostov, and I. D. Rostov (2010), Electronic Atlas of tides of the marginal seas of the Northern Pacific, *Vestnik DVO RAN*, *1*(149), 102–106, (in Russian).

Pichon, A., Y. Morel, R. Baraille, and L. S. Quaresma (2013), Internal tide interactions in the Bay of Biscay: Observations and modelling, *Journal of Marine Systems*, *109–110*, S26–S44, doi:10.1016/j.jmarsys.2011.07.003.

Putov, V. F., and G. V. Shevchenko (1998), Specific features of tidal regime on the northeastern shelf of sakhalin island, in *Hydrometeorological Processes on a Shelf: Impact Assessment on the Marine Environment*, pp. 61–82, DVO RAN, Vladivostok, Russia, (in Russian).

Rabinovich, A. B., and A. E. Zhukov (1984), Tidal fluctuations on the northeastern shelf of Sakhalin Island, *USSR Oceanology*, *24*(2), 238–244, (in Russian).

Rouvinskaya, E., O. Kurkina, A. Kurkin, and A. Zaytsev (2017), Modeling of internal wave action on offshore platforms for hydrological conditions of the Sakhalin shelf zone, *Fundamental and Applied Hydrophysics*, *10*(4), 61–70, doi:10.7868/S2073667317040062.

Rouvinskaya, E. A., D. Y. Tyugin, O. E. Kurkina, and A. A. Kurkin (2018), Mapping of the Baltic Sea by the types of density stratification in the context of dynamics of internal gravity waves, *Fundamentalnaya i Prikladnaya Gidrofizika*, *11*(1), 46–51, doi:10.7868/S2073667318010057.

Rouvinskaya, E. A., O. E. Kurkina, and A. A. Kurkin (2021), Particle transport and dynamic effects during of a baroclinic tidal wave transformation in the conditions of the shelf of the far eastern seas, *Ecological Systems and Devices*, *11*, 109–118, doi:10.25791/esip.11.2021.1270, (in Russian).

Schlitzer, R. (2022), Ocean Data View, https://odv.awi.de/.

Sherwin, T. J., V. I. Vlasenko, N. Stashchuk, D. Jeans, and B. Jones (2002), Along-slope generation as an explanation for some unusually large internal tides, *Deep Sea Research Part I: Oceanographic Research Papers*, *49*(10), 1787–1799, doi:10.1016/s0967-0637(02)00096-1.

Shevchenko, G. V. (1996), Quasi-periodic seasonal variability of tide harmonic constants in the Northwestern Sea of Okhotsk, *Russian Meteorology and Hydrology*, *8*, 50–57.

Stepanov, D. V. (2017), Estimating the baroclinic Rossby radius of deformation in the Sea of Okhotsk, *Russian Meteorology and Hydrology*, *42*(9), 601–606, doi:10.3103/s1068373917090072.

Vlasenko, V., N. Stashchuk, and K. Hutter (2005), *Baroclinic Tides: Theoretical Modeling and Observational Evidence*, Cambridge University Press, Cambridge.

Vlasenko, V., N. Stashchuk, M. E. Inall, and J. E. Hopkins (2014), Tidal energy conversion in a global hot spot: On the 3-D dynamics of baroclinic tides at the Celtic Sea shelf break, *Journal of Geophysical Research: Oceans*, *119*(6), 3249–3265, doi:10.1002/2013jc009708.

Wang, W., R. Robertson, Y. Wang, C. Zhao, Z. Hao, B. Yin, and Z. Xu (2022), Distinct Variability between Semidiurnal and Diurnal Internal Tides at the East China Sea Shelf, *Remote Sensing*, *14*(11), 2570, doi:10.3390/rs14112570.

Zhao, X., Z. Xu, M. Feng, Q. Li, P. Zhang, J. You, S. Gao, and B. Yin (2021), Satellite Investigation of Semidiurnal Internal Tides in the Sulu-Sulawesi Seas, *Remote Sensing*, *13*(13), 2530, doi:10.3390/rs13132530.